SCIENCE CHINA
Information Sciences

• RESEARCH PAPER •

April 2026, Vol. 69, Iss. 4, 142401:1–142401:10
https://doi.org/10.1007/s11432-024-4548-3

2.5 GHz GaN multiple quantum well micro-photodetector for high-speed visible light communication

Yue LIAO†, Xuyang LIU†, Runze LIN, Xugao CUI & Pengfei TIAN*

College of Intelligent Robotics and Advanced Manufacturing, Fudan University, Shanghai 200433, China

Received 2 November 2024/Revised 9 April 2025/Accepted 4 August 2025/Published online 15 January 2026

Abstract This work reported a high-bandwidth GaN multiple quantum wells (MQWs)-based micro-photodetector (PD) with a record modulation bandwidth of 2.5 GHz used as an optical receiver in the visible light communication (VLC) system. We fabricated GaN MQWs-based micro-PDs on the sapphire substrate and investigated the optoelectronic and bandwidth characteristics of the 20 μm micro-PD at high reverse biases. The micro-PD has low background noise at high reverse bias voltages and excellent wavelength selectivity. Then, we tested the VLC systems at different reverse biases by using the orthogonal frequency division multiplexing (OFDM) modulation scheme and a bit-loading algorithm. A data rate of 12.7716 Gbps over a 0.3-m free-space link was demonstrated by the micro-PD at a reverse bias voltage of 70 V. Our work experimentally demonstrates that the GaN MQWs-based micro-PD has excellent optoelectronic characteristics and bandwidth characteristics even at high reverse bias voltages, making it a promising device for high-speed VLC receivers.

Keywords micro-LED, photodetector, visible light communication

Citation Liao Y, Liu X Y, Lin R Z, et al. 2.5 GHz GaN multiple quantum well micro-photodetector for high-speed visible light communication. Sci China Inf Sci, 2026, 69(4): 142401, https://doi.org/10.1007/s11432-024-4548-3

1 Introduction

Recently, a new generation of optoelectronic devices based on III-nitride semiconductor materials has received considerable attention in the industry and academic community [1]. Gallium nitride (GaN), which represents group-III nitride semiconductor materials, exhibits a wider band gap, higher carrier mobility, higher critical breakdown electric field, and smaller dielectric constant compared with the previous two generations of semiconductor materials [2,3]. Therefore, GaN-based photodetectors (PDs) are capable of fulfilling the requirements of the visible light communication (VLC) systems due to their excellent performance, which can withstand a high working voltage and exhibit high modulation bandwidth and exceptional robustness in diverse environments.

Historically, commercial photodetectors based on Si or GaAs have been utilized in VLC systems for signal detection. But their peak sensitivity lies within the near-infrared spectrum, and the broad range of their response spectrum results in increased optical noise [4]. Compared with their Si or GaAs-based counterparts, GaN-based PDs, with the merits of high responsivity, wavelength selectivity, and low dark current, improved the signal-to-noise ratio (SNR) of VLC systems [5].

Several architectures of GaN-based PDs have been proposed, such as metal-semiconductor-metal (MSM) structures [6], p-i-n structures [7, 8], and multiple quantum wells (MQWs) structures [9–15]. Among them, MQWs structures are commonly found in light-emitting diode (LED) structures, so LEDs are proposed to be used as wavelength-selective photodetectors with a response similar to their emission spectrum [9]. Then, a 100 Mbit/s LED-to-LED VLC system was reported using on-off keying (OOK) modulation [10]. However, the transmission rates achieved in VLC systems using LED-based PDs remain limited and fall short of the high-speed requirements of modern VLC applications. Similar to LEDs, micro-LEDs also can be used as photodetectors, offering benefits such as low cost, low dark current, and wavelength selectivity [11], which are proposed as high-speed VLC receivers. In 2018, Ho et al. [12] introduced for the first time GaN MQWs-based micro-photodetectors with a 71.5 MHz bandwidth in VLC systems, achieving a transmission rate of 3.2 Gbps through orthogonal frequency division multiplexing (OFDM) modulation. In 2019, Liu et al. [5] reported a micro-LED array as the PD array in a 350 Mbps multiple-input multiple-output (MIMO) VLC system, employing OOK modulation at −5 V bias. In 2020,

* Corresponding author (email: pftian@fudan.edu.cn)
† These authors contributed equally to this work.

Table 1 Recent achievements of GaN MQWs-based photodetectors.

Year	Bias	PD type	Bandwidth	Modulation format	Data rate	Distance	Reference
2018	−3 V	Single-pixel	71.5 MHz	OFDM	3.2 Gbps	0.5 m fiber and 0.1 m free space	[12]
2019	−5 V	Single-pixel	56.8 MHz	OOK	350 Mbps	1 m free space	[5]
2020	−8 V	Single-pixel	300 MHz	OFDM	7.4 Gbps	1 m free space	[12]
2021	−5 V	In-parallel connection 2×4	228 MHz	OOK	540 Mbps	1.1 m free space	[13]
2022	−20 V	In-parallel connection 4×4	89 MHz	OFDM	10.14 Gbps	1 m free space	[14]
2023	−20 V	In-parallel connection 4×4	–	OFDM	15.26 Gbps	0.5 m free space	[15]
2025	−30 V	Single-pixel	914 MHz	OFDM	12.62 Gbps	0.35 m free space	[16]
2025	−70 V	Single-pixel	2.5 GHz	OFDM	12.77 Gbps	0.3 m free space	This work

a semipolar InGaN/GaN MQWs-based micro-photodetectors fabricated on GaN substrate, featuring a −3 dB bandwidth of 300 MHz, achieved a 7.4 Gbps data rate using OFDM modulation [12]. Recently, MQW-based micro-PDs have been reported to be applied in ultra-high-speed systems with a transmission rate of over 10 Gbps. In 2022, the InGaN/GaN MQW-based micro-PD array enabled a 10.14 Gbps transmission rate in a VLC system using OFDM modulation, with the bandwidth of 89 MHz [14]. In 2023, Xu et al. [15] demonstrated an OFDM VLC system that achieved a transmission rate of 15.26 Gbps by utilizing the MQW-based PD array and post-equalization. The above studies show that GaN MQWs-based micro-PDs are promising for ultra-high-speed VLC systems, and the latest progress in GaN MQWs-based micro-PDs is summarized in Table 1. Most of the aforementioned studies utilized parallel PD arrays as high-speed VLC receivers. Parallel micro-PD arrays can increase the light-receiving surface area, but they also raise the capacitance of the micro-PDs, leading to the reduction of bandwidth and limiting the transmission rate of the systems. In contrast, single GaN-based micro-PDs exhibit lower capacitance and higher bandwidth. By reducing the thickness of the quantum barriers (QB) in the PDs, a single MQWs-based micro-PD achieved a −3 dB bandwidth of 700 MHz [17], indicating the great potential of single MQWs-based micro-PD for high-speed VLC systems. In addition, single GaN MQWs-based micro-PDs have the advantages of smaller size, lower cost, easier integration, and easier fabrication compared with parallel micro-PD arrays, which are considered promising competitors for the development of the multifunctioning system on chip (SoC) [18]. Every single pixel in the micro-LED chip can transmit and receive signals [19–21], which can simplify the architecture of the VLC system, reduce system power consumption, and benefit the realization of MIMO and full-duplex VLC applications. Therefore, it is an important topic to design a single GaN MQWs-based micro-PD with high bandwidth to achieve ultra-high-speed VLC applications and the integration of multifunctional micro-LED devices.

In this paper, we fabricated GaN MQWs-based micro-PDs on the sapphire substrate to explore the prospects of a high-speed GaN-based VLC receiver. Then we analyzed the frequency response limiting factors of GaN MQWs-based micro-PDs and simulated the energy band diagram and electric field. After theoretical analysis, this work explored the optoelectronic and bandwidth characteristics of the 20 μm micro-PD at high reverse bias voltages. Our device exhibited excellent wavelength selectivity with a passband full-width at half-maximum (FWHM) of 49 nm. It also had low background noise and high modulation bandwidth at high reverse bias voltage, which achieved a record bandwidth of 2.5 GHz. Then, we tested the VLC systems by using the OFDM modulation scheme and a bit-loading algorithm at various reverse bias voltages. A single micro-PD served as the optical receiver in the VLC system with a free space transmission distance of 0.3 m, which obtained a maximum transmission rate of 12.7716 Gbps and was below the forward error correction (FEC) threshold of 3.8×10^{-3}. These results demonstrated that the single GaN MQW-based micro-PD is capable of supporting a high-speed VLC system.

2 Device structure and theoretical analysis

2.1 Device fabrication

We fabricated GaN MQWs-based micro-PDs on the sapphire substrate with mesa sizes of 20, 15, 10, and 8 μm. The schematic structure of GaN MQWs-based micro-PD in this work and the transmission electron microscope (TEM) image of the proposed device are shown in Figure 1(a). We used metal-organic chemical vapor deposition (MOCVD) to grow the GaN MQWs-based micro-PD epilayer structures on the conventional c-plane sapphire substrate. The epitaxial wafers of the micro-PD mainly contain a 3.5 μm unintentionally doped GaN layer, a 170 nm strain engineering layer (SEL), a 165.6 nm nine-period $In_{0.202}Ga_{0.798}N$ (2.8 nm)/GaN (15.6 nm) MQWs structure as active region, a 60 nm p-type AlGaN electron blocking layer (EBL) and a 150 nm p-type GaN layer. The indium tin oxide (ITO) film was deposited on the p-type GaN layer as a current spreading layer using magnetron sputtering.

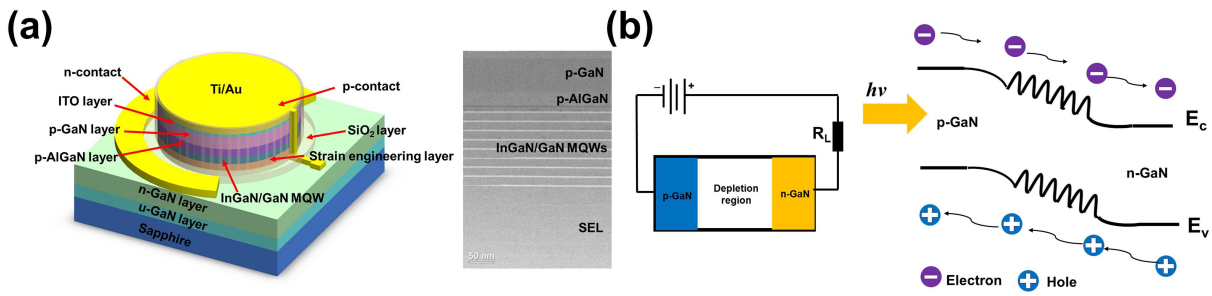

Figure 1 (Color online) (a) Schematic diagram of the GaN MQW-based micro-PD structure. The inset on the right is the cross-sectional TEM image of the epitaxy. (b) The operating schematic diagram and illustrative energy band diagram of the GaN micro-PD under reverse voltage under illumination.

We deposited Ti-Al-Ti-Au on the surfaces of the ITO layer and n-type GaN region to form p-contact and n-contact, respectively. The fabrication process of the GaN MQW-based micro-PD is similar to our previous work [22]. To improve the bandwidth and quantum efficiency of the micro-PD, we grew the strain engineering layer before the MQW growth to further reduce the strain. Similar to normal photodetectors, the GaN MQWs-based micro-PDs are based on a pn junction to achieve photodetection, and the operating schematic diagram and illustrative energy band diagram of micro-PD are demonstrated in Figure 1(b). The working principle of micro-PDs under reverse bias is also exhibited in Figure 1(b). When the light was incident on the surface of the micro-PD, the electron-hole pairs were formed within the depletion region and then were separated by the external electric field. The electrons drifted toward the n-zone and were finally collected in the n-zone, while the holes drifted toward the p-zone and were finally collected in the p-zone. If an external circuit is connected at this time, a photocurrent will be formed.

2.2 Theoretical analysis

To realize high-bandwidth micro-PD, we theoretically analyzed the frequency response limiting factors of GaN MQWs-based micro-PDs. According to the principle of micro-PD described above, the bandwidth is mainly determined by three factors, which are carrier escape lifetime, carrier transit time, and resistance-capacitance (RC) time constant [17]. The carrier transit time is primarily determined by the transit distance and the transit velocity. Therefore, the limited bandwidth of the carrier transit time can be expressed as [23, 24]

$$f_t = \frac{3.5\bar{v}}{2\pi W},$$

$$\frac{1}{\bar{v}^4} = \frac{1}{2}\left(\frac{1}{v_e^4} + \frac{1}{v_h^4}\right),$$

where $\bar{v}$ is the average velocity of carriers, W is the carrier transit distance, v_e is the saturation transit velocity of electrons, and v_h is the saturation transit velocity of holes. Therefore, the carrier transit velocity will affect the bandwidth of the micro-PD, and the carrier transit velocity is associated with the electric field in the device. To investigate the effect of carrier transit velocity on device's bandwidth, the simulated energy band diagram and the electric field of the MQW structure in the proposed micro-PD are demonstrated in Figure 2. Figure 2(a) exhibits the energy band and barrier heights (inset) of the micro-PD at 0 and −11 V. The barrier height in the device at −11 V is lower than that at 0 V. Notably, the internal electric field increases with increasing reverse bias voltage, which can approach 0.8 MV/cm under the reverse voltage of −11 V. The high electric field within the depletion region at −11 V will cause the carriers to travel at velocities approaching their saturation limit [25, 26]. Therefore, the carrier transit time only affects the bandwidth of the proposed micro-PD under low reverse bias voltages, while at high bias voltages, the carrier transit velocity has long been approaching saturation.

Apart from the transit time of the carriers in the depletion region, the bandwidth of a GaN MQWs-based PD also depends on the RC time constant and carrier escape lifetime. The RC-delay bandwidth of micro-PD could be described as

$$f_{RC} = \frac{1}{2\pi RC},$$

$$R \approx R_S + R_L,$$

$$C = \frac{\varepsilon A}{D},$$

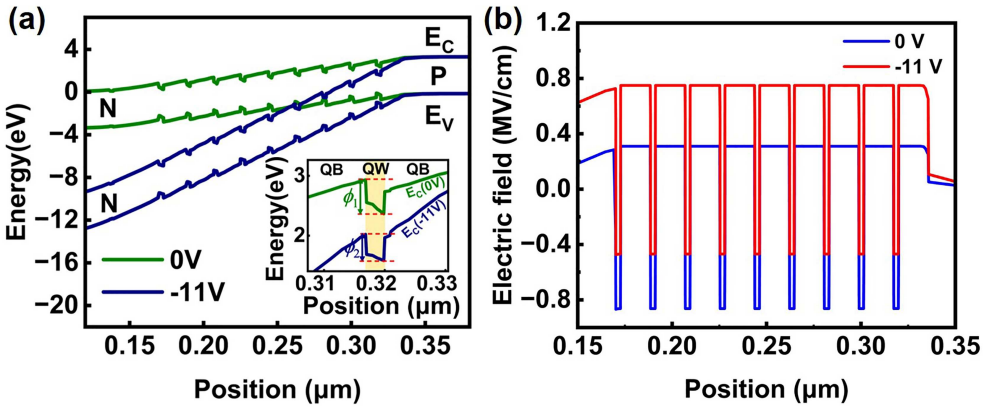

Figure 2 (Color online) (a) The energy band diagrams and barrier heights (inset) of the micro-PD at 0 and −11 V; (b) the electric field diagrams of the micro-PD at 0 and −11 V.

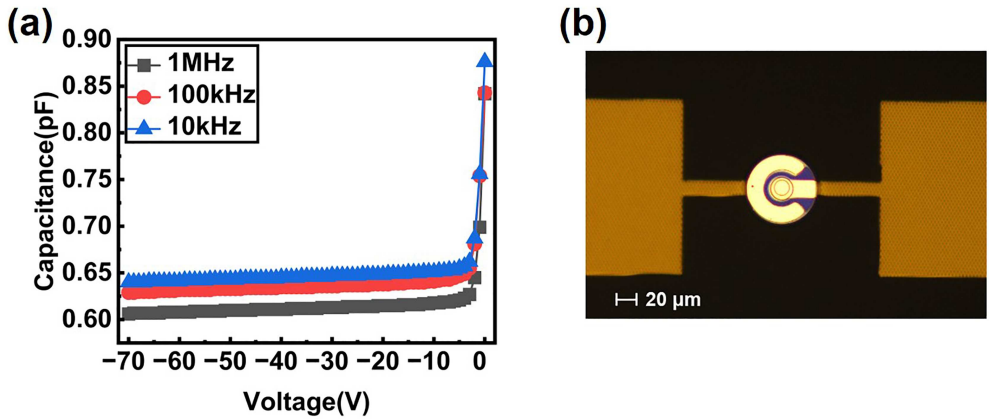

Figure 3 (Color online) (a) The *C*-*V* curves of the micro-PD; (b) the optical microscope image of the 20 μm micro-PD.

where R_S is the series resistance of the micro-PD, R_L is the internal resistance at the receiving end, which is a fixed value of 50 Ω when using a vector network analyzer, C is the junction capacitance of micro-PD, ε is dielectric constant, A is the junction area of the photodetector and D is the width of the depletion layer of the device. According to the above formulas, the RC-delay bandwidth of the proposed micro-PD will be inversely proportional to the capacitance and the resistance of micro-PD. The junction capacitance and resistance can be effectively decreased by decreasing the size of the micro-PD [27]. In addition, a deep etching process in the device fabrication can also reduce the device's capacitance. Then we measured the capacitance-voltage (C-V) curves by using a semiconductor parameter analyzer (Keithley 4200A), which is depicted in Figure 3(a). It can be found that the capacitance of the device declines with increasing reverse voltage. Furthermore, carrier escape lifetime will decrease with increasing reverse bias voltage [28], which demonstrates that the carrier escape lifetime can be effectively shortened by increasing the reverse voltage of micro-PD, thus increasing the modulation bandwidth. From the above theoretical analysis, the micro-PD under high reverse bias has a shorter carrier escape lifetime and smaller capacitance, which results in a higher −3 dB bandwidth. Therefore, we employed a deep etching process in the device fabrication to reduce the device capacitance and chose the 20 μm single micro-PD under high reverse bias voltages to realize the high-speed VLC application, and Figure 3(b) shows the image of the micro-PD with a mesa size of 20 μm.

3 Results and discussion

3.1 Optoelectronic characteristics

We evaluated the optoelectronic characteristics of GaN MQWs-based micro-PD under high reverse voltages. We first explored the spectral response characteristics of the micro-PD as demonstrated in Figures 4(a) and (b). Figure 4(a) shows the current-voltage (I-V) characteristics of the micro-PD, which were measured with wavelengths of 360, 380,

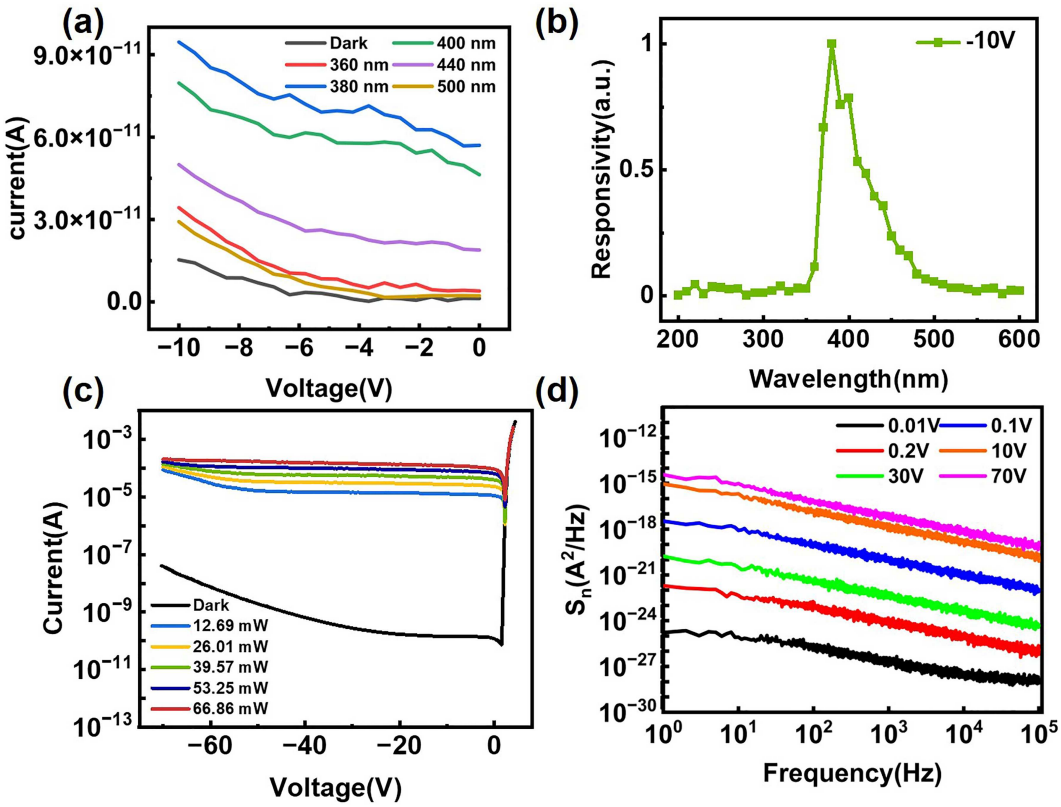

Figure 4 (Color online) (a) *I-V* curves measured in dark conditions and under illumination with various wavelengths of xenon lamp with the incident-optical power density of 37.91 μW/cm^2; (b) the responsivity spectra of the 20 μm micro-PD; (c) *I-V* curves recorded in the dark and under illumination with various incident-optical powers of 405 nm LD; (d) frequency-dependent noise power density of micro-PD under various reverse voltages in dark conditions.

400, 440, and 500 nm as illumination sources with the incident-optical power density of 37.91 μW/cm^2 and under dark conditions, respectively. The monochromatic light of various wavelengths from a xenon lamp (HSX-UV300) illuminated the device passing through a monochromator (Omnno151). It can be found that the photocurrent increases as the wavelength rises from 360 to 380 nm, while it gradually decreases when the wavelength continues to extend to 500 nm. The micro-PD demonstrated a low dark current of 15.3 pA at −10 V and 1.21 pA at 0 V, suggesting that the background noise level is minimal. The results indicate that the photocurrent will increase a lot as the reverse bias voltage rises because more electron-hole pairs are separated and collected at a larger reverse bias voltage resulting in more electrons and holes being extracted from the MQWs.

Figure 4(b) illustrates the responsivity spectrum of the device over the wavelength range from 200 to 600 nm at −10 V. A peak responsivity of 0.066 A/W at −10 V was achieved at a wavelength of 380 nm. The wavelength selectivity of responsivity is from 353 to 460 nm and the FWHM of the micro-PD is 49 nm (367–416 nm), which demonstrates excellent wavelength selectivity of the GaN MQWs-based micro-PD.

To study the photocurrent characteristics of the proposed micro-PD under high reverse voltages, we tested the *I-V* curve of micro-PD over the voltage range from −70 to 4 V, both in darkness and under exposure to different levels of incident optical power from a 405 nm LD, as illustrated in Figure 4(c). The proposed micro-PD exhibits a low dark current even at high bias voltages, with a dark current of 40.4 nA at −70 V, which corresponds to a dark current density of 1.287×10^{-2}A/cm^2. It is evident that the current progressively increases with higher incident optical power density, reaching a maximum of 0.207 mA at −70 V under an incident optical power of 66.86 mW, which corresponds to a current density of 65.92 A/cm^2. Additionally, high photosensitivity is characterized by the ratio of photocurrent to dark current, commonly referred to as the on/off ratio [29]. The on/off ratio is projected to be 104 at high reverse bias voltage and 105 at zero bias, which is mainly because the dark current rises with the reverse voltage. The above results indicate that the proposed micro-PD has a low dark current, proving that it has good weak-signal detectivity. Furthermore, the assessment of weak-signal detectivity quality should also incorporate noise analyses. Although the dark current effectively characterizes the shot noise current, it may not accurately represent the flicker noise current [30]. The noise characteristics of the micro-PD were assessed using a noise measurement analyzer (PDA FS380).

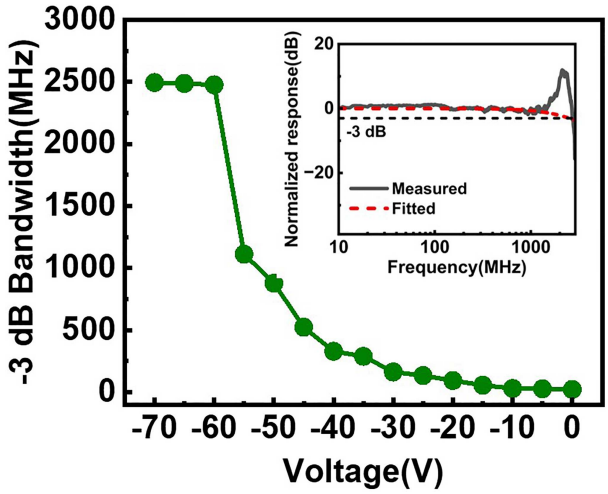

Figure 5 (Color online) The −3 dB bandwidth of micro-PD at different reverse bias voltages. Inset: the measured and fitted data of frequency response of the micro-PD at −70 V.

Figure 4(d) illustrates frequency-dependent noise power density S_n of the GaN MQWs-based micro-PD under the dark condition. The noise of GaN MQWs-based micro-PDs can be divided into three categories, namely "flicker" noise ($1/f$ noise), Johnson noise, and shot noise [5]. It can be found that noise power density at low frequencies is inversely proportional to frequency from Figure 4(d), which indicates that typical $1/f$ noise dominates in the noise of micro-PD at low frequencies. Its noise power density shows a different increasing trend as the reverse bias voltage increases, which is similar to the variation of dark current. These results show that this micro-PD still exhibits excellent optoelectronic characteristics at high reverse bias voltages, which lays the foundation for investigating the communication performance of GaN-based micro-PD under high reverse bias voltages.

3.2 Frequency response characteristics

The modulation bandwidth is an important parameter for evaluating micro-PDs for high-speed VLC systems. The frequency response of the proposed structure was measured under the reverse voltage range of 0 to −70 V using a vector network analyzer (VNA, PicoVNA 106). The proposed device can withstand a maximum reverse bias voltage of 70 V, and avalanche breakdown occurs in the device when the reverse voltage exceeds 70 V. As shown in the inset of Figure 5, the frequency response $P(\omega)$ can be well fitted to the equation [31]:

$$P\left(w\right)=\frac{1}{\sqrt{1+\left(\tau\omega\right)^{2}}},$$

where τ represents the carrier lifetime within the device active region. The −3 dB bandwidth of Figure 5 is read from the fitted frequency response. The modulation bandwidth of the device characterizes how quickly a photodetector converts an optical signal into an electrical signal, defined as the modulation frequency corresponding to a 3 dB drop in the current modulation power of the photodetector. Figure 5 compares the −3 dB bandwidth of the proposed structure under various reverse bias conditions. Observations indicate that the −3 dB bandwidth of the micro-PD is only 22.97 MHz at 0 V, increasing to 2494.8 MHz at −70 V. These test results of bandwidth proved the conclusion of the above theoretical analysis that the −3 dB bandwidth of the device increases as the reverse bias voltage rises. We calculated the slope of the *I*-*V* curve of this device to estimate the series resistance of the device as 43.7 Ω. With the load resistance of 50 Ω and the capacitance of micro-PD that was measured to be 0.606 pF at −70 V, the RC-delay bandwidth was determined to be 2.804 GHz using the appropriate equation. It can be observed that the RC delay bandwidth is similar to the −3 dB bandwidth of micro-PD, indicating that the bandwidth of the proposed micro-PD is primarily limited by the RC delay.

3.3 VLC performances

Figure 6 presents the schematic diagram and photograph of the experimental setup for the VLC system utilizing the 20 μm single micro-PD. At the transmitter, alternating current (AC) signals generated by an arbitrary waveform generator (AWG, Keysight M8190A) were amplified by an electrical amplifier (EA, Mini-Circuits ZFL-2500VH+)

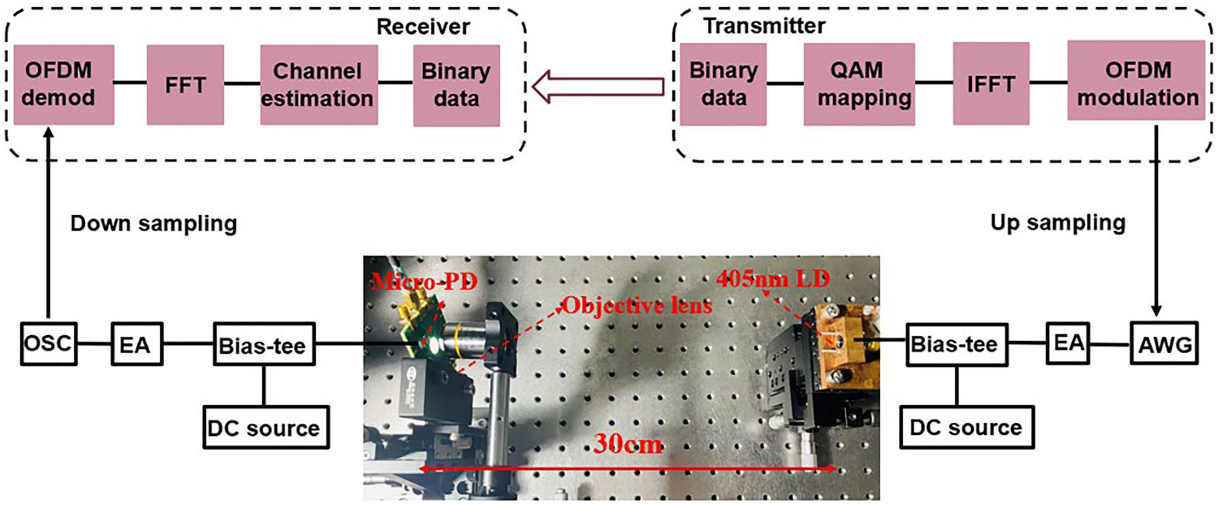

Figure 6 (Color online) The schematic diagram and the experimental photograph of the free-space VLC system utilizing the micro-PD.

and combined with direct current (DC) by a bias-tee (Mini-Circuits ZFBT-6GW+) to drive a 405 nm LD (Thorlabs, L405P150). Then, the light emitted from LD was collimated and focused using a lens and an objective lens (Olympus PLN10X/0.25) before being transmitted over a free-space distance of 0.3 m. The 405 nm LD was modulated using the OFDM modulation scheme, and an OFDM signal was generated via the MATLAB program. The modulated light was aligned with the 20 μm micro-PD at the receiver, which can achieve optical-to-electrical (O/E) conversion. At the receiver, the micro-PD was connected to a bias-tee (Mini-Circuits ZFBT-6GW+), providing reverse voltages. The signal received from the micro-PD was amplified using an electrical amplifier (EA, Mini-Circuits ZHL-2-12+) before being transmitted to an oscilloscope (OSC, Agilent DSA90604A). Subsequently, the data acquired from the OSC was demodulated offline. Furthermore, we also measured the *I*-*V* characteristics and frequency response of micro-PD using the setup as shown in Figure 6.

To enhance the spectral efficiency (SE) of the VLC system, we further implemented a bit-power loading algorithm in the experiment. First, the SNR of each subcarrier was estimated by transmitting the quadrature phase shift keying (QPSK) signal as a training signal. Next, the binary data was first mapped into a quadrature amplitude modulation (QAM) format of varying orders after serial-to-parallel (S/P) conversion. The orders of QAM were calculated using the Levin-Campello (LC) algorithm based on the estimated SNR and the target bit error rate (BER) threshold [32]. After up-sampling at 2x and inverse fast Fourier transform (IFFT), the real-value signal was obtained by Hermitian symmetry. Finally, after parallel to serial (P/S) conversion and adding the cyclic prefix (CP), the signal was converted into time-domain OFDM symbols before being sent to AWG. For the receiver module, the signal from OSC was resampled and processed by removing CP, FFT, and down-sampling to convert a frequency-domain signal. Then, channel estimation based on the least squares (LS) algorithm was employed to reduce the impact of channel fading response. Finally, after QAM demapping and parallel-to-serial conversion, the binary data was recovered, allowing for the calculation of the bit error rate (BER), SNR, and SE. The data rate could be calculated from the product of the signal modulation bandwidth and SE [33].

The above results show that the micro-PD at the reverse bias voltage of 70 V exhibited a larger photocurrent and modulation bandwidth compared to other bias voltages, thereby facilitating the transmission of high-frequency signals. We investigated the VLC performance of the proposed device at the reverse bias voltage of 70 V. We initially established the optimal driving current of LD and signal peak-to-peak voltage (V_{PP}) for the proposed micro-PD is 160 mA and 0.8 V, respectively. Subsequently, we assessed the SNR of each subcarrier by transmitting the OFDM BPSK signal as a training signal and calculated the bit number using the LC algorithm.

Figure 7 shows the VLC performance of the proposed device at −70 V. Figure 7(a) illustrates SNR distribution and bit allocation on subcarriers of the channel. The average SE, derived from the bit loading results, can attain a value of 6.3858 bits/s/Hz. One can observe that although the average SNR is 22.7425 in the range of 0–2 GHz, the SNR is only 10 dB at 100 MHz and almost 4 dB at 1.8 GHz, which means that the signal in these frequency ranges can be difficult to demodulate at the receiver. It is evident that the data rate reaches up to 12.7716 Gbps at −70 V under the FEC threshold of 3.8×10^{-3} as shown in Figure 7(b). This represents the highest data rate achieved by a single GaN-MQWs-based micro-PD. Meanwhile, refinements in the lens architecture in optics have been implemented. After lens optimization, the data rate of the proposed device and the transmission distance

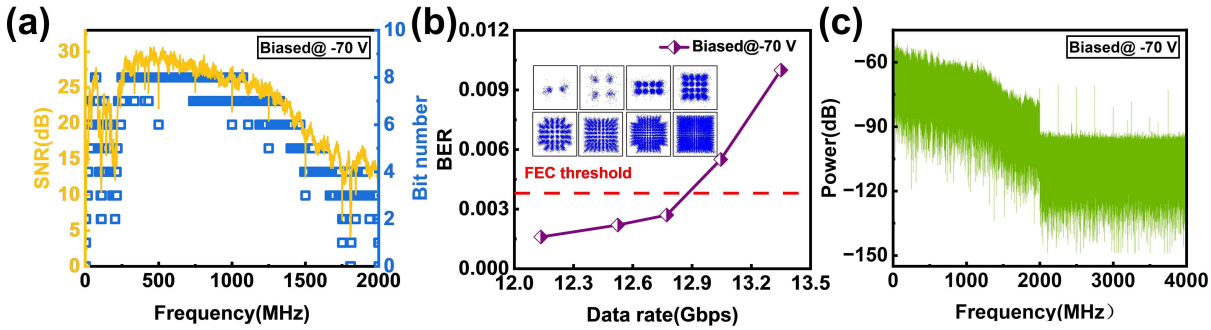

Figure 7 (Color online) (a) The SNR distribution and bit allocation of the VLC system using the proposed micro-PD; (b) BER versus data rate and constellation plots of the VLC system; (c) the power spectrum of the OFDM signal.

Table 2 Comparison of VLC performance of the single micro-PD under different reverse bias voltages.

	−10 V	−30 V	−50 V	−70 V
Photocurrent (mA)	0.124	0.149	0.173	0.207
−3 dB bandwidth (MHz)	31.0	163.6	878.8	2494.8
SE (bit·s^{-1}·Hz^{-1})	5.9860	6.4569	6.6186	6.3858
Signal bandwidth (MHz)	250	1000	1500	2000
Data rate (Gbps)	1.4965	6.1569	9.9279	12.7716
Average SNR (dB)	22.0526	22.5412	23.4400	22.7425
BER	0.0038	0.0038	0.0025	0.0027

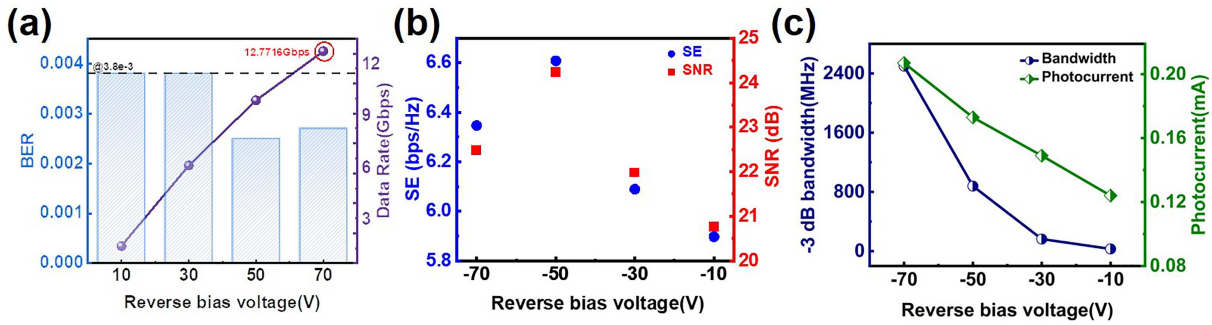

Figure 8 (Color online) (a) The BER and data rate versus reverse bias voltages of the VLC system based on the micro-PD; (b) the average SE and average SNR versus reverse bias voltages; (c) the −3 dB bandwidth and photocurrent of the micro-PDs versus reverse bias voltage under the incident-optical power of 66.86 mW of 405 nm LD.

can be further improved. The OFDM signal power spectrum is illustrated in Figure 7(c), which shows the signal bandwidth of micro-PD at −70 V is 2000 MHz, due to the limitation of the AWG in the VLC system.

To examine the impact of reverse voltages applied to the proposed device on VLC performance, we tested the communication performance of the proposed device under different reverse voltages in the same optical path. We summarized the VLC performance of the single micro-PD at various reverse voltages in Table 2 and Figure 8. Figure 8(a) illustrates the BER and data rate versus reverse voltages. The date rates of the VLC systems are 1.4965, 6.1569, 9.9279, and 12.7716 Gbps at the reverse bias voltage of 10, 30, 50, and 70 V, respectively. We summarized the average SE and average SNR versus reverse voltage as illustrated in Figure 8(b). The observed trend of the average SE with reverse bias voltage is analogous to that of the average signal-to-noise ratio SNR, and the device at −50 V has the highest average SNR and SE. Figure 8(c) shows the −3 dB bandwidth and photocurrent versus reverse bias voltage curves under the incident-optical power of 66.86 mW of 405 nm LD. It is evident that both the photocurrent and modulation bandwidth of the micro-PD increase with rising reverse bias voltage, which can enable higher data rates to be achieved at a higher reverse bias voltage. The results presented above demonstrated the significant potential of single GaN-MQWs-based micro-PDs as optical signal receivers in high-speed VLC links.

4 Conclusion

In conclusion, through device structural and fabrication process optimization, we have developed a device capable of withstanding a high bias voltage of −70 V while achieving a record bandwidth of 2.5 GHz. We analyzed bandwidth limiting factors of GaN MQWs-based micro-PD, which showed that the capacitance and carrier escape lifetimes of the device decreased when reverse bias voltage increased, thereby increasing the modulation bandwidth. Therefore, we examined the optoelectronic properties, bandwidth characteristics, and VLC performance of GaN MQWs-based micro-PD at high reverse bias voltages. The GaN MQWs-based micro-PD has excellent optoelectronic performance, which still maintains low background noise at high reverse bias voltage. Then, we presented a high-speed visible light communication (VLC) system that utilized a single GaN MQWs-based micro-PD, employing the OFDM modulation scheme along with a bit-loading algorithm. In the VLC system, this high-bandwidth micro-PD was employed to obtain a data rate approaching 13 Gbps over a free space transmission distance of 0.3 m satisfying the FEC requirements. This work highlighted the significant potential of GaN MQWs-based micro-PDs for ultra-high-speed VLC applications exceeding 10 Gbps. In addition, this high-speed micro-PD can be seamlessly integrated with a high-speed micro-LED to implement a multifunctional integrated chip, applicable to MIMO or full-duplex VLC systems, reducing system complexity and enabling higher data rates.

Acknowledgements This work was supported by National Key Research and Development Program of China (Grant No. 2021YFB3601003).

References

1 Alshehri B, Dogheche K, Belahsene S, et al. Dynamic characterization of III-nitride-based high-speed photodiodes. IEEE Photonics J, 2017, 9: 1–7
2 Ferreyra R A, Zhu C, Teke A, et al. Group III nitrides. In: Springer Handbook of Electronic and Photonic Materials. Berlin: Springer. 2017
3 Yang X, Li J C, Peng X H, et al. Super retina TFT based full color microLED display via laser mass transfer. Sci China Inf Sci, 2024, 67: 210401
4 Lu T W, Huang Y, Lai S Q, et al. Full-duplex visible light communication system based on single blue mini-LED acting as transmitter and photodetector simultaneously. J Lightw Technol, 2023, 41: 2639–2649
5 Liu X, Lin R, Chen H, et al. High-bandwidth InGaN self-powered detector arrays toward MIMO visible light communication based on micro-LED arrays. ACS Photonics, 2019, 6: 3186–3195
6 Walker D, Monroy E, Kung P, et al. High-speed, low-noise metal-semiconductor-metal ultraviolet photodetectors based on GaN. Appl Phys Lett, 1999, 74: 762–764
7 Butun B, Tut T, Ulker E, et al. High-performance visible-blind GaN-based pin photodetectors. Appl Phys Lett, 2008, 92: 033507
8 Huang H, Yan D, Wang G, et al. GaN-based p-i-n ultraviolet photodetectors with a thin p-type GaN layer on patterned sapphire substrates. Chin Opt Lett, 2014, 12: 092301
9 Miyazaki E, Itami S, Araki T. Using a light-emitting diode as a high-speed, wavelength selective photodetector. Rev Sci Instrument, 1998, 69: 3751–3754
10 Stepniak G, Kowalczyk M, Maksymiuk L, et al. Transmission beyond 100 Mbit/s using LED both as a transmitter and receiver. IEEE Photon Technol Lett, 2015, 27: 2067–2070
11 Lin R, Liu X, Zhou G, et al. InGaN micro-LED array enabled advanced underwater wireless optical communication and underwater charging. Adv Opt Mater, 2021, 9: 2002211
12 Ho K T, Chen R, Liu G, et al. 32 Gigabit-per-second visible light communication link with InGaN/GaN MQW micro-photodetector. Opt Express, 2018, 26: 3037–3045
13 Chang Y H, Hsu T C, Liou F J, et al. High-bandwidth InGaN/GaN semipolar micro-LED acting as a fast photodetector for visible light communications. Opt Express, 2021, 29: 37245–37252
14 Shi J, Xu Z, Niu W, et al. Si-substrate vertical-structure InGaN/GaN micro-LED-based photodetector for beyond 10 Gbps visible light communication. Photon Res, 2022, 10: 2394–2404
15 Xu Z, Luo Z, Lin X, et al. 15.26Gb/s Si-substrate GaN high-speed visible light photodetector with super-lattice structure. Opt Express, 2023, 31: 33064–33076
16 Shen D, Ren T, Chen X, et al. Bandwidth optimization of GaN-MQW photodetectors for visible light communication via deep etching and bias voltage control. Opt Laser Technol, 2025, 183: 112223
17 Chow Y C, Lee C, Wong M S, et al. Dependence of carrier escape lifetimes on quantum barrier thickness in InGaN/GaN multiple quantum well photodetectors. Opt Express, 2020, 28: 23796–23805
18 Gao X, Jia B, Ye Z Q, et al. Simultaneous transmission, detection, and energy harvesting. Opt Lett, 2021, 46: 2075–2078
19 Huang Y M, Peng C Y, Miao W C, et al. High-efficiency InGaN red micro-LEDs for visible light communication. Photon Res, 2022, 10: 1978–1986
20 Huang W T, Peng C Y, Chiang H, et al. Toward high-bandwidth yellow-green micro-LEDs utilizing nanoporous distributed Bragg reflectors for visible light communication. Photon Res, 2022, 10: 1810–1818

21 Chang Y H, Huang Y M, Liou F J, et al. 2.805 Gbit/s high-bandwidth phosphor white light visible light communication utilizing an InGaN/GaN semipolar blue micro-LED. Opt Express, 2022, 30: 16938–16946

22 Lin R, Jin Z, Qiu P, et al. High bandwidth series-biased green micro-LED array toward 6 Gbps visible light communication. Opt Lett, 2022, 47: 3343–3346

23 Kato K. Ultrawide-band/high-frequency photodetectors. IEEE Trans Microwave Theor Techn, 2002, 47: 1265–1281

24 Kato K, Hata S, Kawano K, et al. Design of ultrawide-band, high-sensitivity pin protodetectors. IEICE Trans Electron, 1993, 76: 214–221

25 Bellotti E, Bertazzi F. Transport parameters for electrons and holes. In: Nitride Semiconductor Devices: Principles and Simulation. Hoboken: Wiley, 2007

26 Ji D, Ercan B, Chowdhury S. Experimental determination of velocity-field characteristic of holes in GaN. IEEE Electron Device Lett, 2019, 41: 23–25

27 Pulfrey D L, Kuek J J, Leslie M P, et al. High UV/solar rejection ratios in GaN/AlGaN/GaN p-i-n photodiodes. IEEE Trans Electron Device, 2002, 48: 486–489

28 Lang J R, Young N G, Farrell R M, et al. Carrier escape mechanism dependence on barrier thickness and temperature in InGaN quantum well solar cells. Appl Phys Lett, 2012, 101: 181105

29 Zhan Z, Zheng L, Pan Y, et al. Self-powered, visible-light photodetector based on thermally reduced graphene oxide-ZnO (rGO-ZnO) hybrid nanostructure. J Mater Chem, 2012, 22: 2589–2595

30 McKendry J J D, Massoubre D, Zhang S, et al. Visible-light communications using a CMOS-controlled micro-light- emitting-diode array. J Lightwave Technol, 2011, 30: 61–67

31 Jiang Z X, Wu Z Y, Ma C C, et al. P-type β-Ga_2O_3 metal-semiconductor-metal solar-blind photodetectors with extremely high responsivity and gain-bandwidth product. Mater Today Phys, 2020, 14: 100226

32 Campello J. Practical bit loading for DMT. In: Proceedings of IEEE International Conference on Communications, 1999. 801-805

33 Hu F, Chen S, Li G, et al. Si-substrate LEDs with multiple superlattice interlayers for beyond 24 Gbps visible light communication. Photon Res, 2021, 9: 1581–1591